Inorganic Chemistry

Article

pubs.acs.org/IC

Synthesis, Characterization, and Photophysics of Oxadiazole- and Diphenylaniline-Substituted Re(I) and Cu(I) Complexes

Raphael Horvath,[†] Michael G. Fraser,[†] Scott A. Cameron,[†] Allan G. Blackman,[†] Pawel Wagner,[‡] David L. Officer,[‡] and Keith C. Gordon*[,†]

[†]MacDiarmid Institute for Advanced Materials and Nanotechnology, Department of Chemistry, University of Otago, Dunedin, New Zealand

[‡]ARC Centre of Excellence for Electromaterials Science, Intelligent Polymer Research Institute, University of Wollongong, Australia

Supporting Information

ABSTRACT: Transition-metal complexes of the types $[Re(CO)_3Cl(NN)]$, $[Re(CO)_3py(NN)]^+$, and $[Cu(PPh_3)_2(NN)]^+$, where NN = 4,4′-bis(5-phenyl-1,3,4-oxadiazol-2-yl)-2,2′-bipyridine (OX) and 4,4′-bis(*N*,*N*-diphenyl-4-[ethen-1-yl]-aniline)-2,2′-bipyridine (DPA), have been synthesized and characterized. Crystal structures for $[Re(CO)_3Cl(DPA)]$ and $[Cu(PPh_3)_2(OX)]BF_4$ are presented. The crystal structure of the rhenium complex shows a trans arrangement of the ethylene groups, in agreement with density functional theory calculations. The structure of the copper complex displays the planar aromatic nature of the bpy−oxadiazole ligand. Density functional theory modeling of the complexes was supported by comparison of calculated and experimental normalized Raman spectra; the mean absolute deviations of the complexes were <10 cm^{-1}. The Franck−Condon state was investigated using UV−vis and resonance Raman spectroscopic as well as density functional theory computational techniques. It was shown that the lowest energy absorption peaks are metal to ligand charge transfer and ligand-centered charge transfer for the oxadiazole- and diphenylaniline-substituted bipyridine ligands, respectively. The lowest energy excited states were characterized using transient emission and absorption spectroscopic techniques in conjunction with density functional theory calculations. These showed that the DPA complexes had ligand-centered nonemissive "dark" states with lifetimes ranging from 300 to 2000 ns.

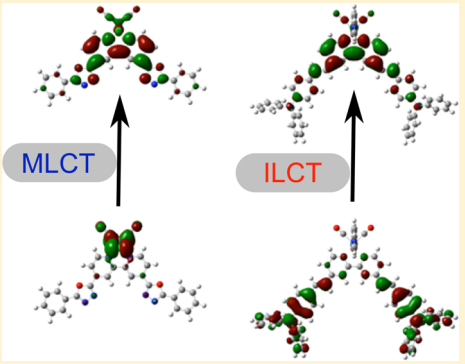

INTRODUCTION

Metal polypyridyl complexes, such as $[Ru(bpy)_3]^{2+}$, $[Re(CO)_3Cl(bpy)]$, and $[Cu(PPh_3)_2(bpy)]^+$ (bpy = 2,2′-bipyridine) and their derivatives, have been studied for applications such as solar energy conversion or display technologies[1−8] due to the presence of low-energy ^{3}MLCT (metal-to-ligand charge transfer) states. Consequently, the ground and excited-state electronic structures, dipoles, and associated vibrational modes of $[Re(CO)_3Cl(bpy)]$, $[Cu(PPh_3)_2(bpy)]^+$, and related compounds are relatively well studied and known.[1,9−12] By appropriate functionalization, these complexes can be used to effect charge separation by photolysis or act as emissive centers under application of a potential. To this end, electron-withdrawing and -donating groups such as oxadiazoles and diphenylanilines are often appended to metal complexes to induce electron- and hole-transporting properties, respectively. Oxadiazole-substituted complexes[3,13,14] and complex polymers[15] have been investigated for their use in electroluminescent and sensitizing applications. A number of groups have substituted ruthenium-based solar cell dyes with diphenylanilines, attached via ethenyl linkers, in order to improve the solar absorption profiles.[16−20] In every case this induced strong absorption bands at ca. 420−500 nm; however, these remain largely unassigned. Correct understanding of the photophysical properties that these substituents may induce is crucial in designing useful functional materials. While the $\{Re(CO)_3Cl\}$ moiety has been shown to be electron withdrawing,[21] in $[Cu(PPh_3)_2(bpy)]^+$ and related compounds, the level of communication between the copper(I) and the ligand is relatively low. For MLCT transitions, the radical anion of the ligand can in theory be observed with little interference from the metal. Furthermore, in contrast to Ru(II)-based complexes, little interference from ancillary ligands is expected. This makes both Re(I) and Cu(I) complexes excellent reference compounds to ascertain the effects of the aforementioned substituents on the ground and excited-state electronic properties of metal−polypyridyl complexes.

This work examines the effect of substitution of 2,2′-bipyridine ligands at the 4,4′ positions by electron-withdrawing oxadiazole and electron-donating diphenylaniline substituents to give the 4,4′-bis(5-phenyl-1,3,4-oxadiazol-2-yl)-2,2′-bipyridine (OX) and 4,4′-bis(*N*,*N*-diphenyl-4-[ethen-1-yl]-aniline)-2,2-bipyridine (DPA) ligands, which are shown in Figure 1. Complexes investigated were $[Re(CO)_3Cl(NN)]$, $[Re(CO)_3py(NN)]^+$, and $[Cu(PPh_3)_2(NN)]^+$ (where NN = bpy,

Received: August 22, 2012

   dx.doi.org/10.1021/ic3018387 | *Inorg. Chem.* XXXX, XXX, XXX−XXX

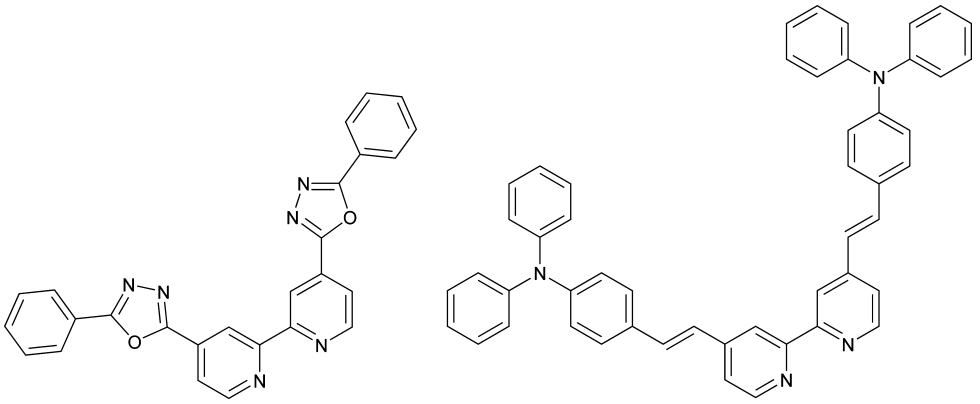

4,4'-bis(5-phenyl-1,3,4-oxadiazol-2-yl)-2,2'-bipyridine (OX)

4,4'-bis(N,N-diphenyl-4-[ethen-1-yl]-aniline)-2,2'-bipyridine (DPA)

Figure 1. OX and DPA ligands used to synthesize complexes $[Re(CO)_3Cl(NN)]$, $[Re(CO)_3py(NN)]^+$, and $[Cu(PPh_3)_2(NN)]^+$.

OX, or DPA and py = pyridine). Resonance Raman spectroscopy, transient emission, and ground- and excited-state absorption spectroscopic techniques were used. Density functional theory (DFT) optimization and frequency calculations were carried out at the 6-31G(d)/LANL2DZ level to aid assignment of vibrational modes in the resonance Raman spectra; their accuracies were verified using FT-IR and FT-Raman spectroscopic techniques. Furthermore, time-dependent (TD) DFT calculations in a solvent field have been used to quantify electronic transitions using both the B3LYP and the CAM-B3LYP functionals.

EXPERIMENTAL SECTION

Synthesis. All commercially available reagents were used as received. The ligands OX (4,4′-bis(5-phenyl-1,3,4-oxadiazole)-2,2′-bipyridine) and DPA (4,4′-bis(2-(4-diphenylaminophenyl))-2,2′-bipyridine) were prepared by literature methods.[13,15,22]

All metal complexes were synthesized by established literature techniques with minor variations.[12,23] The precursor $[Cu(PPh_3)_4]BF_4$ was synthesized by the method of Rader et al.[24]

[Re(CO)$_3$Cl(OX)]. A 0.100 g amount of OX (0.225 mmol) and 0.082 g of $Re(CO)_5Cl$ (0.225 mmol) were refluxed for 7 h in 30 mL of ethanol under N_2. The resulting orange solution was refrigerated overnight. The orange solid was filtered to give the analytically pure solid. Yield: 0.157 g (0.209 mmol, 93%). ^{1}H NMR ($CDCl_3$, 400 MHz): δ 7.60−7.69 (m, 6H, phenyl), 8.21−8.28 (m, 6H, phenyl and bpy overlapping), 9.09 (s, 2H, bpy), 9.30 (d, 2H, J = 6 Hz, bpy). Anal. Calcd for $C_{29}H_{16}N_6O_5ClRe$: C, 46.43; H, 2.15; N, 11.21. Found: C, 46.51; H, 2.24; N, 11.08. ESI POS: m/z 773 {([$Re(CO)_3Cl(OX)$] + Na^+)}.

[Re(CO)$_3$py(OX)]PF$_6$. A 0.15 g amount of $[Re(CO)_3Cl(OX)]$ (0.2 mmol) and 0.051 g of $AgPF_6$ (0.2 mmol) were refluxed in 50 mL of acetonitrile under N_2 in the dark for 18 h. The resulting yellow solution was filtered through Celite to remove the AgCl precipitate. A 10 mL amount of saturated aqueous NH_4PF_6 was added to the filtrate. Acetonitrile was then removed under reduced pressure. The yellow solid (0.16 g) was filtered and washed with water. The solid, assumed to be $[Re(CO)_3(CH_3CN)OX]PF_6$, was reacted to form the pyridine adduct without characterization. A 0.16 g amount of $[Re(CO)_3(CH_3CN)OX]PF_6$ (0.18 mmol) and 0.445 g of pyridine (5.63 mmol) were refluxed in 50 mL of methanol for 4 h. The resulting solution was reduced in volume to 25 mL under reduced pressure and refrigerated overnight. The resulting yellow solid was filtered and recrystallized from methanol. Yield: 0.14 g (0.149 mmol, 75% overall). ^{1}H NMR ($(CD_3)_2CO$, 400 MHz): δ 7.5 (m, 2H, py), 7.7 (m, 6H, bpy and py overlapping), 8.03 (t, ^{1}H, py), 8.28 (dd, 4H, J_1 = 7 Hz, J_2 = 1 Hz, phenyl), 8.681 (m, 4H, bpy and py overlapping), 9.63 (s, 2H, bpy), 9.80 (d, 2H, J = 6, bpy). Anal. Calcd for $C_{34}H_{21}N_7O_5RePF_6$: C, 43.50; H, 2.26; N, 10.45. Found: C, 43.32; H, 2.43; N, 10.27. ESI POS: m/z 793.74 {($Re(CO)_3py(OX))^+$}.

[Cu(PPh$_3$)$_2$(OX)]BF$_4$. Dry diethyl ether (20 mL) was purged with nitrogen for 10 min. $[Cu(PPh_3)_4]$ BF_4 (0.363 g, 0.337 mmol) and OX (0.150 g, 0.337 mmol) were added, and the suspension was stirred under N_2 for 48 h. The yellow precipitate was filtered and washed with diethyl ether and recrystallized from a minimum amount of methanol. Yield: 0.200 g (0.178 mmol, 53%). Crystals of suitable quality for X-ray crystallography were grown by slow diffusion of diethyl ether into a concentrated dichloromethane solution. ^{1}H NMR ($CDCl_3$, 400 MHz): δ 7.10−7.75 (m, 34H), 8.26 (dd, 2H, J_1 = 5 Hz, J_2 = 1 Hz), 8.36 (m, 6H), 8.66 (m, 2H), 9.14 (s, 2H). Anal. Calcd for $C_{62}H_{46}N_6O_2P_2CuBF_4$: C, 65.47; H, 4.25; N, 7.39. Found: C, 65.23; H, 4.00; N, 7.22. ESI POS: m/z 769.15 {($Cu(PPh_3)(OX)^+$)}.

[Re(CO)$_3$Cl(DPA)]. A 0.100 g amount of DPA (0.144 mmol) and 0.052 g of $[Re(CO)_5Cl]$ (0.144 mmol) were refluxed for 7 h in 30 mL of ethanol under N_2. The resulting red solution was refrigerated overnight. The red solid was filtered to give analytically pure solid. Yield: 0.126 g (0.127 mmol, 88%). ^{1}H NMR: ($CDCl_3$, 400 MHz) δ 6.72 (d, 2H, J = 16 Hz, ethenyl), 7.01−7.19 (m, 20H), 7.30−7.35 (m, 8H), 7.53 (d, 2H, J = 16 Hz, ethenyl), 7.58 (d, 2H, J = 6 Hz), 8.28 (s, 2H, bpy), 8.58 (d, 2H, J = 6 Hz, bpy). Anal. Calcd for $C_{53}H_{38}N_4O_3ClRe$: C, 63.62; H, 3.83; N, 5.60. Found: C, 63.51; H, 4.05; N, 5.63. ESI POS: m/z 983.25 {($Re(CO)_3(DPA) + H_2O)^+$}, 965.24 {$Re(CO)_3(DPA)^+$}.

[Re(CO)$_3$py(DPA)]PF$_6$. A 0.1 g amount of $[Re(CO)_3Cl(DPA)]$ (0.1 mmol) and 0.025 g of $AgPF_6$ (0.20 mmol) were refluxed in 50 mL of acetonitrile under N_2 in the dark for 18 h. The resulting red solution was filtered through Celite to remove the AgCl precipitate. A 10 mL amount of saturated aqueous NH_4PF_6 was added to the filtrate. Acetonitrile was then removed under reduced pressure. The resulting red solid (0.1 g) was filtered and washed with water. The solid, assumed to be $[Re(CO)_3(CH_3CN)DPA]PF_6$, was reacted to form the pyridine adduct without characterization. A 0.1 g amount of $[Re(CO)_3(CH_3CN)(DPA)]PF_6$ (0.09 mmol) and 0.200 g of pyridine (2.61 mmol) were refluxed in 30 mL of methanol for 4 h. The solution was reduced in volume to 25 mL under reduced pressure and subsequently refrigerated overnight. The red solid was filtered and washed with water. A 10 mL amount of $NH_4PF_{6(aq)}$ was added to the filtrate to precipitate further product. Yield: 0.082 g (0.068 mmol, 68% overall). ^{1}H NMR ($(CD_3)_2CO$, 400 MHz): δ 7.01 (d, 4H, J = 8 Hz, phenyl), 7.16 (m, 12H, phenyl), 7.30 (d, 2H, J = 16 Hz, ethenyl), 7.37 (m, 8H, phenyl), 7.52 (m, 2H, py), 7.6 (d, 4H, J = 8 Hz, phenyl), 7.87 (d, 2H, J = 16 Hz, ethenyl), 8.03 (m, 3H, bpy and py overlaid), 8.60 (m, 2H), 8.87 (s, 2H, bpy), 9.28 (d, 2H, J = 6 Hz, bpy). Anal. Calcd

dx.doi.org/10.1021/ic3018387 | Inorg. Chem. XXXX, XXX, XXX−XXX

for $C_{58}H_{43}N_5O_3RePF_6$: C, 58.58; H, 3.65; N, 5.89. Found: C, 58.25; H, 3.48; N, 5.93. ESI POS: m/z 1044.15 {$(Re(CO)_3py(DPA))^+$}.

[Cu(PPh$_3$)$_2$(DPA)]BF$_4$ MeOH. Dry diethyl ether (20 mL) was purged with nitrogen for 10 min. $[Cu(PPh_3)_4]BF_4$ (0.231 g, 0.215 mmol) and DPA (0.150 g, 0.215 mmol) were added, and the suspension was stirred under N_2 for 48 h. The orange precipitate was filtered and washed with diethyl ether and recrystallized from a minimum amount of methanol. Yield: 0.194 g (0.142 mmol, 66%). ^{1}H NMR ($CDCl_3$, 400 MHz): δ 7.04−7.17 (m, 30H), 7.19−7.24 (m, 10H), 7.28−7.37 (m, 16H), 7.57−7.64 (m, 8H), 8.11 (d, 2H, J = 5 Hz), 8.73 (s, 2H). Anal. Calcd for $C_{86}H_{68}N_4P_2CuBF_4$: C, 74.54; H, 5.18; N, 4.00. Found: C, 74.42; H, 4.96; N, 3.99. ESI POS: m/z 1019.32 {$(Cu(PPh_3)(DPA)^+)$}.

Measurements. Crystal structures of $[Cu(PPh_3)_2(OX)]^+$ and $[Re(CO)_3Cl(DPA)]$ were acquired with a Bruker diffractometer equipped with an Apex II charge-coupled device (CCD) area detector using graphite-monochromated Mo Kα (λ = 0.71073 Å) radiation. Data collection parameters are listed in Table 1. Structures were solved by direct methods and refined on F^2 by use of all data in full-matrix least-squares procedures. All non-hydrogen atoms were refined with anisotropic displacement parameters. Hydrogen atoms were included in calculated positions with isotropic displacement parameters 1.2 times the isotropic equivalent of their carrier carbon atoms. Included in the structure of $[Cu(PPh_3)_2(OX)]BF_4$ are one molecule of $CHCl_3$ solvent and a single BF_4^- counteranion per cation. The completeness of the $[Cu(PPh_3)_2(OX)]BF_4$ structure is 94% due to data collection in a monoclinic unit cell rather than the correct symmetry, triclinic. However, the data are of high quality. FT-IR spectra were acquired in solid-state KBr disks as 64 coadded scans using a Perkin-Elmer BX FT-IR spectrometer. FT-Raman data were acquired using a Bruker Equinox 55 interferometer coupled with a FRA-106 Raman module and a D418T liquid-nitrogen-cooled germanium detector, controlled by the Bruker OPUS v5.5 software package. Spectra were acquired as 1024−2048 coadded scans using 1064 nm radiation of a Nd:YAG laser operating at 450 mW. The resolution for both FT-IR and FT-Raman spectra is 4 cm^{-1}. For absorption, emission, and lifetime measurements, ca. 10^{-5} mol L^{-1} CH_2Cl_2 solutions were used. These were argon purged for 20 min before spectral acquisition to remove any dissolved gases. UV−vis absorption spectra were acquired with a Jasco V-550 spectrophotometer. Steady-state emission spectra were acquired with a Perkin-Elmer LS-50 B luminescence spectrometer using an excitation wavelength of 350 nm. Excited-state emission and absorption transients were acquired using a LP920K transient absorption (TA) system (Edinburgh Instruments). Excitation was carried out using pulsed third-harmonic radiation (355 nm) from a Brilliant (Quantel) Nd:YAG laser operating at 5 Hz, and in TA mode a Xe900 450W xenon arc lamp was used as the probe source. Photons were dispersed using a TMS300-A monochromator with a 1800 grooves/mm grating, recorded on a R928 (Hamamatsu) photomultiplier and transcribed on a TDS3012C (Tektronix) oscilloscope.[25] Fluorescence correction was applied for the transient absorption spectra as part of the optical density (ΔOD) calculation. An exponential decay curve was fitted to the output to obtain the lifetime. Samples were in CH_2Cl_2 solution and thoroughly degassed using argon prior to the experiment. Temperature was controlled using a TLC 50/E (Quantum Northwest Inc.) sample holder. Resonance Raman measurements were performed using the setup described in detail by Howell et al.[26,27] A continuous-wave Innova I-302 krypton-ion laser (Coherent, Inc.) was used for excitation wavelengths λ_{ex} of 350.7, 406.7, and 413.1 nm, a diode-pumped laser (CrystaLaser) for λ_{ex} = 444.3 nm, and a Melles Griot OmNichrome model 543-MAP argon laser at λ_{ex} = 488.0 and 514.5 nm. The sample and collection lens were arranged in a 135° backscattering geometry, and the Raman photons were focused on the entrance slit of an Acton Research SpectraPro500i spectrograph with a 1200 grooves mm^{-1} grating. Signal was recorded using a liquid-nitrogen-cooled Spec-10:100B CCD controlled by WinSpec/32 software (Roper Scientific), operating at −100 °C. A similar system but using a 300 grooves mm^{-1} grating and a temperature-controlled Flash 300 (Quantum Northwest, Inc.) sample holder was used to collect temperature-dependent emission data.

Computational Modeling. Frequency and time-dependent (TD) calculations were performed on the optimized ground-state structures. All calculations were performed using the B3LYP method, except the TD calculations, which were additionally performed using CAM-B3LYP. The latter were carried out using the Gaussian 09 package (Gaussian, Inc.), while all B3LYP calculations were carried out using Gaussian 03 (Gaussian, Inc.). All calculations used the 6-31G(d) basis set for the ligands, while heavy metal centers were approximated using a LANL2DZ effective core potential.[25,28,29] TD calculations were performed under CH_2Cl_2 solvent fields implemented with the IEF polarizable continuum (PCM) model, while other calculations were performed without a solvent model. The effective peak center for calculated electronic transitions was determined as an average weighted by constituent oscillator strengths. For $[Cu(PPh_3)_2(DPA)]^+$ the PPh_3 groups were approximated with PH_3 in order to achieve a reasonable computational time. The output frequencies were scaled to minimize the mean actual deviations (MADs) between calculated and experimental peaks by a factor of approximately 0.975.[30] IR and

Table 1. Crystal Data and Structure Refinement for $[Cu(PPh_3)_2(OX)]BF_4$ and $[Re(CO)_3Cl(DPA)]$

	$[Cu(PPh_3)_2(OX)]BF_4$	$[Re(CO)_3Cl(DPA)]$
empirical formula	$C_{63}H_{47}BCl_{13}CuF_4N_6O_2P_2$	$C_{53.17}H_{38.33}C_{l1.33}N_4O_3Re$
fw	1238.71	1014.68
temp.	89(2) K	89(2) K
wavelength	0.71069 Å	0.71073 Å
cryst syst	triclinic	trigonal
space group	$P\bar{1}$	$R\bar{3}$
unit cell dimens	a = 11.6160(10) Å	a = 40.2046(13) Å
	b = 14.3910(14) Å	b = 40.2046(13) Å
	c = 19.589(3) Å	c = 14.0107(6) Å
	α = 103.990(5)°	α = 90°
	β = 96.298(5)°	β = 90°
	γ = 108.619(3)°	γ = 120°
volume	2948.3(6) Å^3	19 612.9(12) Å^3
Z	2	18
density (calcd)	1.395 Mg/m^3	1.546 Mg/m^3
abs coeff	0.623 mm^{-1}	2.920 mm^{-1}
F(000)	1268	9216
cryst size	0.38 × 0.24 × 0.15 mm^3	0.40 × 0.20 × 0.20 mm^3
θ range for data collection	1.09−25.50°	2.12−25.35°
index ranges	$-11 \le h \le 13$	$-48 \le h \le 48$
	$-17 \le k \le 16$	$-48 \le k \le 48$
	$-23 \le l \le 22$	$-16 \le l \le 16$
no. of reflns collected	62 816	107 101
no. of independent reflns	9936 [$R_{(int)}$ = 0.0449]	7974 [$R_{(int)}$ = 0.0963]
completeness to θ	(25.00°) 93.50%	(25.35°) 99.9%
abs corr	semiempirical from equivalents	semiempirical from equivalents
max and min transmission	1.000000 and 0.833427	0.5928 and 0.3880
refinement method	full-matrix least-squares on F^2	full-matrix least-squares on F^2
data/restraints/params	9936/0/739	7974/92/599
goodness-of-fit on F^2	1.053	1.071
final R indices [$I > 2\sigma(I)$]	R_1 = 0.0432, wR_2 = 0.1037	R_1 = 0.0885, wR_2 = 0.1778
R indices (all data)	R_1 = 0.0593, wR_2 = 0.1169	R_1 = 0.1256, wR_2 = 0.1998
largest diff. peak and hole	0.729 and −0.544 e·Å^{-3}	3.641 and −2.119 e·Å^{-3}

dx.doi.org/10.1021/ic3018387 | Inorg. Chem. XXXX, XXX, XXX−XXX

Raman spectra were generated using a Lorentzian line shape with a half-width at half-maximum (HWHM) of 3 cm^{-1}. Vibrational modes and molecular orbitals (MOs) were visualized using Molden[31] and GaussView v4.1 (Gaussian, Inc.), respectively, after extraction from the output files using GaussSum.[32]

RESULTS AND DISCUSSION

Crystal Structures. Crystals of $[Re(CO)_3Cl(DPA)]$ of suitable quality for X-ray crystallography were grown from vapor diffusion of diisopropyl ether into a dichloromethane solution of the complex. The structure is shown in Figure 2

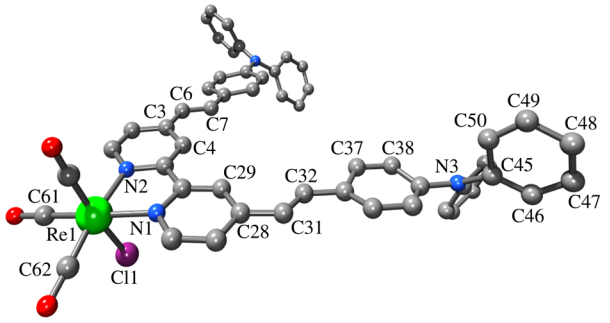

Figure 2. POVRAY perspective view of $[Re(CO)_3Cl(DPA)]$. Disordered solvent molecules and hydrogen atoms are omitted for clarity.

with the solvent and counterion removed for clarity, and selected bond lengths and angles are presented in Table 2. The

Table 2. Bond Lengths (Angstroms) and Angles (degrees) for the Crystal Structures Described

$[Re(CO)_3Cl(DPA)]$			
Re1−C62	1.8562(7)	Re1−C61	1.9151(4)
Re1−C60	1.9122(8)	Re1−N2	2.1311(3)
Re1−N1	2.178(9)	Re1−Cl1	2.480(3)
N2−Re1−N1	75.4(4)	C62−Re1−C61	85.3(6)
C62−Re1−C60	92.2(6)	C61−Re1−C60	88.5(6)
$[Cu(PPh_3)_2(OX)]^+$			
Cu1−N1	2.063(2)	Cu1−P1	2.2295(8)
Cu1−N2	2.071(2)	Cu1−P2	2.2520(8)
N1−Cu1−N2	80.16(8)	N1−Cu1−P2	101.74(6)
N1−Cu1−P1	116.62(6)	N2−Cu1−P2	107.51(6)
N2−Cu1−P1	110.94(6)	P1−Cu1−P2	129.00(3)

[a]For four-coordinate complexes, τ_4 can be used to establish a quantitative measure of how close a geometry is to tetrahedral (τ_4 = 1), trigonal pyramid (τ_4 = 0:85), square planar (τ_4 = 0). $\tau_4 = \{360° - (\Theta + \theta)/141°$ (Θ and θ are the two largest bond angles of the tetrahedron).

complex crystallized in the trigonal space group $R\bar{3}$. Eighteen complex molecules comprise the unit cell, as well as three highly disordered dichloromethane solvent molecules, which are located on symmetry sites. This was modeled with each dichloromethane molecule disordered over six sites. The SQUEEZE function identifies a 40-electron hole, consistent with this. The $\{Re(CO)_3Cl\}$ fragment displays bond lengths and angles consistent with a distorted octahedral geometry, with the N1−Re1−N2 angle of 75.4°. A mean plane through the atoms of the bpy moiety and a mean plane through the Re and the equatorial carbonyl carbons (C61 and C62) lie at an angle of 16.14°. This shows the bpy ligand bent out of the Re−carbonyl equatorial plane. The N1−Re1−Cl1 angle of 81.78° is also consistent with a distorted octahedral geometry. This is not uncommon for complexes of the type $[Re(CO)_3(L)Cl]$, where L = polypyridyl. A search of the Cambridge structural database of *fac*-$[Re(CO)_3Cl(bpy)]$-based complexes gives 33 results with a mean N−Re−Cl bond angle of 84.463°. Similarly, the same analysis carried out on 16 *fac*-$[Re(CO)_3Cl(phen)]$-based (phen =1,10-phenanthroline) complexes gives a mean N−Re−Cl angle of 84.413°. This is partly due to the size of the rhenium ion which forces it to sit out of the plane of the bpy or phen ligands.

The crystal structure displays a trans,trans arrangement of the ethylene groups. This is consistent with ^1H NMR spectroscopy, where J = 16 Hz is observed for the ethylene protons (vide supra) and is consistent with the lowest energy geometry calculated by DFT. Two rotamers are possible for the trans ethylene groups with respect to their orientation to the bpy moiety. Rotation of the C3−C6−C7 angle 180° around the C3−C6 bond is possible and likewise rotation of the C28−C31−C32 angle 180° around the C31−C32 bond. The structure in Figure 3 shows an "inward−inward" (rotamer A) orientation of the ethylene groups, i.e., C7 and C32 are eclipsed with C4 and C29, respectively. Other possibilities are that both ethylene groups are pointing "outward" (rotamer C) or one ethylene group is pointing in and the other out (rotamer B). Structures of the related complexes, {4,4′-bis[*p*-diethylamino)-*α*-styryl]-2,2′-bipyridine}tricarbonylchlororhenium(I)[33] and (4,4′-distyryl-2,2′-bipyridine)tricarbonyl acetonitrilerhenium(I) tetrafluoroborate[34] both show a "inward−outward" orientation of the ethylene groups (rotamer B). It should be noted that rotamer C has been calculated as the lowest energy form and thus likely corresponds to the species predominantly present in solution.

The outer phenyl ring (C45−C50) is disordered over two sites. Atoms labeled C45−C50 in Figure 2 have 60% occupancy. Rotation of the phenyl ring around the N3−C45 bond of 29.88° results in the remaining 40% occupancy (these atoms are not shown in Figure 2). C37 and C38 of the styryl phenyl ring are also disordered over two sites with a 60/40 occupancy. The two halves of the DPA ligand are twisted slightly from planarity. Relevant distortion angles between the pyridyl ring and the phenyl rings range from 170.1° to 178.43°, indicating slight nonplanarity, enough to retain conjugation through the bpy ligand. Within the crystal, molecules of $[Re(CO)_3Cl(DPA)]$ form dimers; a depiction of this can be found in Figure S1 (Supporting Information). The shortest of the intermolecular H−Cl contacts is 2.726°. A similar dimer formation is observed in the related complex {4,4′-bis[*p*-diethylamino)-*α*-styryl]-2,2′-bipyridine}-tricarbonylchlororhenium(I).[33] This intermolecular interaction may be facilitating formation of rotamer A in the crystal.

Crystals of $[Cu(PPh_3)_2(OX)]BF_4$ were grown from vapor diffusion of diethyl ether into a chloroform solution. A diagram of the complex cation is shown in Figure 4, and selected bond lengths and angles are presented in Table 2. Crystallization occurred with a noncoordinating tetrafluoroborate anion and a chloroform solvent molecule in the triclinic space group $P\bar{1}$. As found for many $[Cu(I)(PPh_3)_2(NN)]^+$ complexes (NN = diimine ligand), the Cu(I) metal center displays a distorted tetrahedral geometry and the P−Cu−P angle of 129° and the N−P−N angle of 80.16° exemplify this distortion. A substructure search of the Cambridge structural database of $[Cu(I)(PPh_3)_2(bpy)]^+$ compounds result in 16 complexes, with

dx.doi.org/10.1021/ic3018387 | Inorg. Chem. XXXX, XXX, XXX−XXX

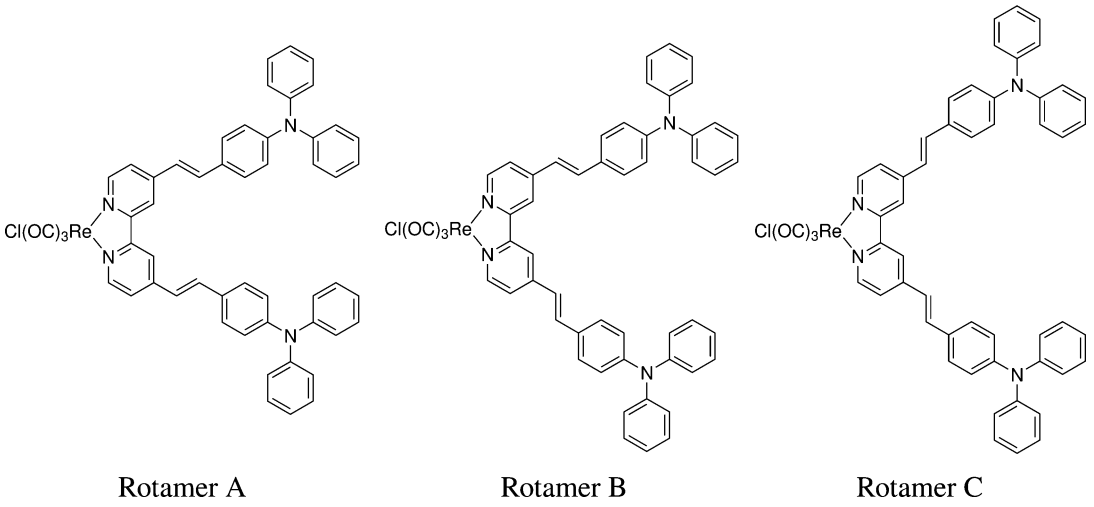

Figure 3. Possible rotamers of $[Re(CO)_3Cl(DPA)]$.

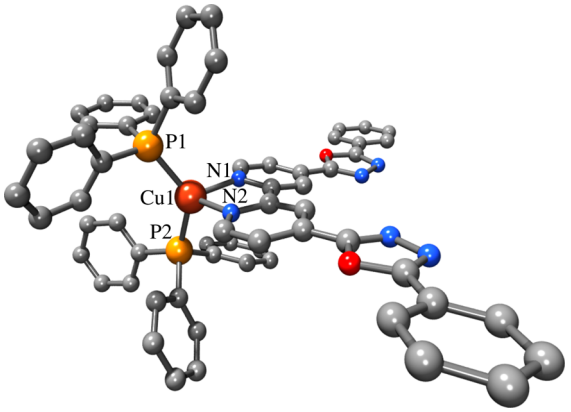

Figure 4. POVRAY perspective view of the $[Cu(PPh_3)_2(OX)]^+$ cation. BF_4^- counteranion and hydrogen atoms are omitted for clarity.

a mean P−Cu−P angle of 120.7° and a mean N−Cu−N angle of 78.4°. The geometry index τ_4* = 0.81, consistent with a trigonally distorted tetrahedron.[35] The OX ligand can be treated as two halves, each half consisting of a pyridyl, oxadiazole, and phenyl ring (py−Ox−Ph). Each half of the ligand displays only small deviations from planarity. The planes between the py and the Ox sections are 7.3° and 5.9° to one another for the sides of the ligand bonded to the Cu through N1 and N2, respectively. The pyridyl rings of the OX ligand are twisted by 10.67° to each other.

Ground-State Vibrational Spectra. The C≡O stretching frequencies (Table 3) of $[Re(CO)_3Cl(OX)]$ are subtly but consistently higher than those of $[Re(CO)_3Cl(DPA)]$. This is due to decreased back-bonding from the ligand π_L^* orbitals to the C≡O antibonding orbitals via the metal dπ system and thus consistent with the electron-withdrawing properties of the oxadiazole unit. This trend is well represented in computational spectra; however, the agreement between calculated and observed peak positions is less than optimal (vide infra). The wavenumber of the high-frequency C≡O stretch of $[Re(CO)_3Cl(bpy)]$ lies between that of the OX and DPA compounds; however, the low-frequency C≡O stretches are at significantly lower wavenumbers. Other significant features in the FT-IR spectra are due to phenyl- or bipyridine-related vibrations.

Table 3. Carbonyl Stretching Frequencies of the Rhenium Complexes[a]

	$\tilde{\nu}$(CO)/cm^{-1}		
symmetry	$a'(2)$	a''	$a'(1)$
$[Re(CO)_3Cl(bpy)]$		1883	2019
$[Re(CO)_3Cl(OX)]$	1902	1923	2026
$[Re(CO)_3Cl(DPA)]$	1897	1919	2016
$[Re(CO)_3py(bpy)]^+$[b,c]		1950	2040
$[Re(CO)_3py(OX)]^+$		1938	2034
$[Re(CO)_3py(DPA)]^+$		1922	2030

[a]Symmetry assignments are from ref 11. [b]From ref 12. [c]In CH_2Cl_2.

FT-Raman spectra of the OX- and DPA-containing complexes are shown in Figure 5. For reference, spectra of $[Re(CO)_3Cl(bpy)]$ and $[Cu(PPh_3)_2(bpy)]^+$ are shown in Figure S2 (Supporting Information). All complexes feature spectra that are dominated by delocalized vibrations, corresponding to aromatic ring deformations. The vibrational modes of the OX- and DPA-substituted compounds can be identified both from comparison to the bipyridine complexes and calculated vibrational spectra. Marked peaks correspond to modes that are significant in resonance Raman spectra and will be further discussed below.

IR and Raman vibrational stretching frequencies and intensities can be calculated with reasonable accuracy for transition-metal complexes using DFT at the 6-31G(d) level for ligands and LANL2DZ level for heavy atoms.[28] As IR and Raman spectroscopic techniques are concerned with the electronic dipole and polarizability, respectively, good spectral correlation gives confidence to the calculated values of these and related quantities, such as structure, vibrational modes, and energetics.[25,30] Mean absolute deviations (MADs) were determined as they provide a way to quantitatively monitor the accuracy of the peak wavenumbers in a calculated spectrum.[36] These data were calculated by averaging the absolute difference in wavenumbers of the most prominent experimental peaks to the corresponding calculated peaks in the spectral range from 400 to 1800 cm^{-1} and are shown in Table S1 (Supporting Information). Each spectrum was scaled to minimize the MADs. The average of the MAD values obtained is <7 cm^{-1}, and the assignment of vibrational peaks is definitely possible from the calculated spectra. Carbonyl stretching peaks

dx.doi.org/10.1021/ic3018387 | Inorg. Chem. XXXX, XXX, XXX−XXX

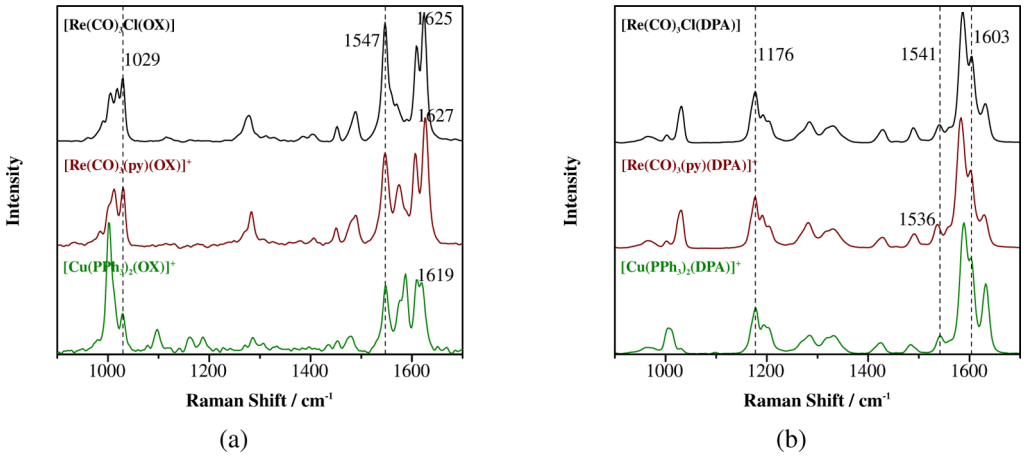

Figure 5. FT-Raman spectra acquired in a KBr disk. (a) Complexes containing the OX ligand; (b) complexes containing the DPA ligand.

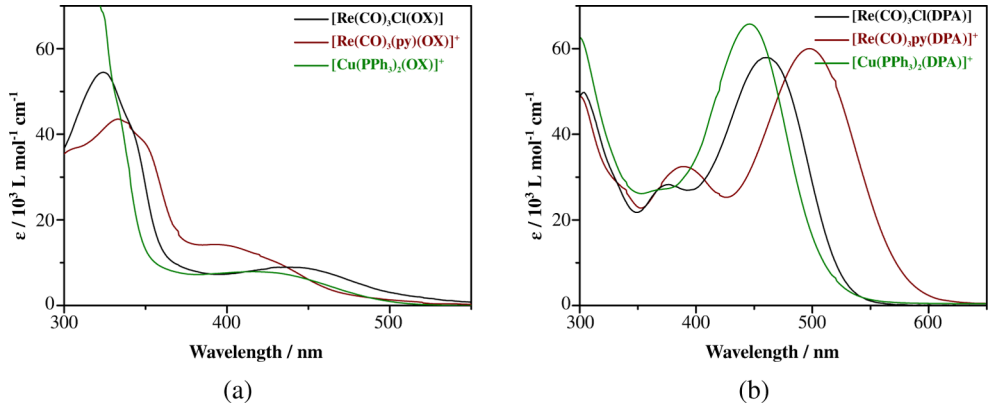

Figure 6. Electronic absorption spectra acquired in CH_2Cl_2. (a) Complexes containing the OX ligand; (b) complexes containing the DPA ligand.

were not included in the calculations, as they require different scale factors;[37] however, as they are spectrally isolated from other features, their vibrational modes are straightforward to assign nevertheless.

Electronic Absorption Spectroscopy. Electronic absorption spectra of the OX- and DPA-based complexes in CH_2Cl_2 are shown in Figure 6a and 6b, respectively, and the observed peaks, along with the electronic transitions calculated using the B3LYP and CAM-B3LYP functionals, are summarized in Table 4. The energies and shapes of the highest occupied and lowest unoccupied molecular orbitals (HOMOs and LUMOs, respectively) are shown in Figure 7 and presented in Table 5; additional MOs can be found in Table S2 (Supporting Information).

The lowest energy transitions of $[Re(CO)_3Cl(OX)]$ and $[Re(CO)_3Cl(DPA)]$ are both calculated as HOMO−1/HOMO → LUMO, where LUMO signifies bpy-based orbitals in the complexes (see Table 5); however, their origins vary significantly. The oxadiazole-substituted complex is calculated to behave much like unsubstituted $[Re(CO)_3Cl(bpy)]$ in that the lowest energy transition is MLCT in nature, followed by $\pi \rightarrow \pi^*$ transitions at higher energies. These transitions are red shifted compared to the unsubstituted complex, which can be attributed to a stabilization of the π_L^* acceptor orbital, as shown in Figure 7. Metal-based dπ orbitals appear relatively unaffected in comparison. The absorption spectrum of $[Re(CO)_3Cl(DPA)]$ shows a strong band at 460 nm. For this complex the electron-rich nature of the diphenylaniline substituents effects an increase in the energies of the ligand π_L orbitals, causing them to become the new HOMOs, as shown in Figure 7. The π_L^* energy appears unchanged with respect to $[Re(CO)_3Cl(bpy)]$. This gives rise to an electron shift from diphenylaniline to bpy that is best described as a ligand-centered charge transfer (LCCT). As visible from the MO pictures in Table 5, this transition also contains significant $\pi \rightarrow \pi^*$ character due to overlap of the donor and acceptor orbitals. Two sets of transitions are calculated for this peak in B3LYP (see Table 4), which differ in whether the transitions terminate on the LUMO or LUMO+1 orbitals. For the former, the transition energy is significantly underestimated, which is not unexpected for charge transfer transitions calculated using this functional.[38] Using CAM-B3LYP as the functional leads to a single set of transitions but at a slightly overestimated energy. This method has been designed to compensate for the shortcomings in the long-range modeling of charge transfer transitions of B3LYP.[38,39] The higher energy $\pi \rightarrow \pi^*$ transitions on the other hand are better approximated with the B3LYP functional.

Compared to $[Re(CO)_3Cl(OX)]$, the lowest energy absorption peak of $[Re(CO)_3py(OX)]^+$ is blue shifted by ca. 40 nm while $[Re(CO)_3py(DPA)]^+$ shows a red shift of ca. 20 nm. These effects can both be explained by the relative electron-withdrawing influence of the py ligand compared to Cl^-. The most significant effect of this is a stabilization of the metal dπ set of orbitals, which is of significantly greater extent than that of bpy-based π_L and π_L^* orbitals, leading to an increase in the HOMO−LUMO gap of the material (see Figure 7).

dx.doi.org/10.1021/ic3018387 | Inorg. Chem. XXXX, XXX, XXX−XXX

Table 4. UV−Vis Absorption Data Correlated to TD-DFT-Calculated Electronic Transitions Using the B3LYP and CAM-B3LYP Functionals in a CH_2Cl_2 Solvent Field[a]

	expt.	B3LYP		CAM-B3LYP	
	λ/nm (ε/M^{-1} cm^{-1})	λ/nm (f)	transition[a]	λ/nm (f)	transition[a]
$[Re(CO)_3Cl(bpy)]$	386 (3.7)[a]	405 (0.071)	H → L	336 (0.099)	H−1, H → L
$[Re(CO)_3Cl(OX)]$	437 (9.0)	473 (0.183)	H−1, H → L	376 (0.265)	H−1, H → L
	338sh (44.2)	378 (1.054)	H−4 to H → L, L+1	307 (1.492)	H−4, H−3, H−1 → L, L+1
	324 (54.5)	321 (0.753)	H−9, H−7 to H−2 → L, L+1	298 (0.600)	H−4, H → L, L+1
$[Re(CO)_3Cl(DPA)]$	460 (57.9)	554 (1.174)	H−1, H → L	399 (3.083)	H−3, H−1, H → L, L+1
		442 (1.293)	H−1, H → L+1		
	376 (28.3)	351 (0.563)	H−5 to H−2 → L, L+1	350 (0.113)	H−3 to H → L, L+1
	303 (49.7)				
$[Re(CO)_3py(bpy)]^+$	366 (24.0) [b]	365 (0.103)	H−2, H−1 →	334 (0.100)	H−2, H−1 → L
$[Re(CO)_3py(OX)]^+$	393 (14.2)	416 (0.986)	H−3, H → L	363 (0.144)	H−2, H → L
	347sh (39.0)	373 (0.036)	H−4, H−3 → L	344 (0.513)	H−3, H−1 → L
	333 (43.5)	353 (0.737)	H−1, H → L+1	316 (1.373)	H−2, H → L, L+1
	306 (36.6)	321 (0.385)	H−7, H−4 to H−1 → L to L+2	299 (0.441)	H−4, H−3, H → L, L+1
$[Re(CO)_3py(DPA)]^+$	479 (60.0)	594 (1.289)	H−1, H → L	429 (3.284)	H−1, H → L, L+1
		456 (1.543)	H−1, H → L+1		
	389 (32.5)	394 (0.470)	H−4, H → L, L+3	267 (0.587)	H−6, H → L, L+2
$[Cu(PPh_3)_2(bpy)]^+$	356 [c]	382 (0.089)	H−2 to H → L	292 (0.129)	H−1, H → L
$[Cu(PPh_3)_2(OX)]^+$	415 (7.9)	463 (0.208)	H → L	333 (0.360)	H−4, H → L
	333sh (46.7)	368 (0.146)	H → L+1		
$[Cu(PPh_3)_2(DPA)]^+$	446 (65.7)	515 (1.354)	H−1, H → L	390 (3.353)	H−1, H → L, L+1
		428 (1.348)	H−1, H → L+1		
	368 (26.9)	373 (0.227)	H−1, H → L+2	294 (0.238)	H−2 to H → L to L+2

[a]H and L refer to highest occupied molecular orbitals and lowest unoccupied molecular orbitals respectively. [a]The dominant orbital contributions are shown.

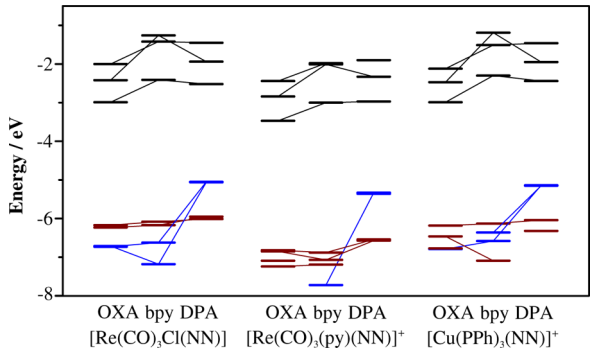

Figure 7. Energies of the frontier MOs of all complexes, as calculated by B3LYP. Red shades correspond to metal-based occupied MOs while blue shades correspond to ligand-based occupied MOs. All virtual orbitals shown are π_L^*. Complexes with bpy ligands are included for comparison.

Diphenylamine-based π_L and π_L^* orbitals on the other hand are too distant to experience significant inductive effects from py, which, coupled with the energy decrease of bpy π_L^* orbitals, decreases the energy of the charge transfer transition taking place. As with the $[Re(CO)_3Cl(NN)]$ complexes, CAM-B3LYP underestimates transition energies; generally predictions are somewhat more accurate than those made using B3LYP. Both methods appear to calculate enhanced mixing of dπ and π_L orbitals, which is most likely related to the aforementioned decrease in dπ orbital energy. This sometimes makes it difficult to classify MOs as "ligand based" or "metal based".

The copper complexes exhibit a number of similar transitions, albeit at different energies. As shown in Figure 7, the occupied orbitals have been calculated to be of similar energies as those of the respective $[Re(CO)_3Cl(NN)]$ complexes, that is, the ionization energies are expected to be similar. $[Cu(PPh_3)_2(OX)]^+$ shows MLCT transitions as a peak at 425 nm and a shoulder at 333 nm on a strong PPh_3 absorption to the blue edge of the window. The ligand-based charge transfer transition of $[Cu(PPh_3)_2(DPA)]^+$ is blue shifted to 446 nm compared to the rhenium complexes; the involved acceptor orbitals appear in analogous locations to those of the rhenium complexes. The difference in energy can be attributed to an increase in the energies of the virtual orbitals, reflecting a lack of stabilization by the comparatively innocent copper metal. Again, B3LYP and CAM-B3LYP functionals under- and overestimate the MLCT transition energies, respectively, while the higher energy $\pi \rightarrow \pi^*$ transitions are adequately described by B3LYP.

Resonance Raman (RR) Spectroscopy. If Raman spectroscopy is carried out with incident light (λ_{ex}) of similar energy to an electronic transition of the analyte, resonance enhancement is observed of specific peak intensities, namely, those corresponding to normal modes that mimic the change in equilibrium bond lengths (ΔQ) upon electronic excitation.[40] This enables the activity in a particular part of the molecule for a given λ_{ex} to be determined and thus correlated to an electronic transition.[36] Although the change in intensity means that direct comparison of calculated spectra to RR spectra is difficult, comparison is possible via FT-Raman spectra as they show identical peak positions. Resonance Raman spectra of the rhenium and copper complexes are shown in Figures 8 and 10, respectively. In order to obtain a satisfactory signal-to-noise ratio at long wavelengths, spectra of $[Re(CO)_3Cl(OX)]$ and $[Re(CO)_3Cl(DPA)]$ were acquired in DMSO, where higher concentrations could be achieved compared to CH_2Cl_2, which was used for the remaining complexes.

dx.doi.org/10.1021/ic3018387 | Inorg. Chem. XXXX, XXX, XXX−XXX

Table 5. MO Diagrams of the [Re(CO)$_3$Cl(NN)] Complexes[a]

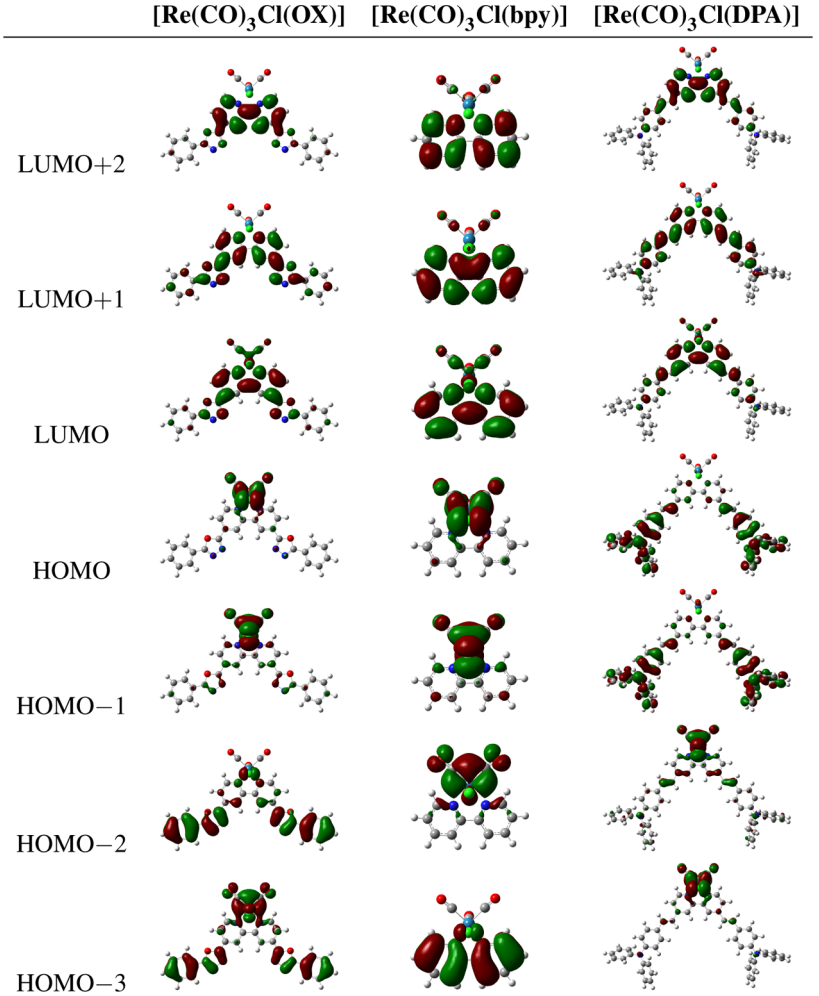

[a]The orbitals correspond to calculations carried out in a CH_2Cl_2 solvent field using B3LYP.

At long wavelengths, [Re(CO)$_3$Cl(OX)] shows resonance enhancement for the peaks at 1028, 1283, 1486, and 1628 cm^{-1}. The peak at 1028 cm^{-1} has been assigned as corresponding to a vibration delocalized over the entire ligand, while the other peaks correspond to vibrations localized on the bpy portion of the ligand. Most significantly, however, the fully symmetric carbonyl stretch at 2022 cm^{-1} is visible in all spectra; it is usually the most intense peak, with the exception of the λ_{ex} = 350.7 nm spectrum. This supports the assignment of the lowest energy electronic absorption peak as ^{1}MLCT, as such a transition would cause a significant change in the equilibrium C≡O bond length. At λ_{ex} = 350.7 nm some of these peaks diminish in intensity, although they are still visible. Peaks at 1548 and 1608 cm^{-1} have been assigned as delocalized and oxadiazole based and display an increase in intensity in the resonance Raman spectra. This is consistent with resonance with a $\pi \rightarrow \pi^*$ transition; the peak is centered at 324 nm in the absorption spectrum.

Similar spectra are observed for the complex [Re(CO)$_3$py(OX)]$^+$ (Figure 8c). Due to strong fluorescence, spectra with λ_{ex} > 457.9 nm show a low signal-to-noise ratio and are therefore omitted. The most obvious difference with respect to the [Re(CO)$_3$Cl(NN)] complex is a red shift of the C≡O stretch to 2040 cm^{-1}, as discussed for the FT-Raman spectra. The similarity of the spectra to those of [Re(CO)$_3$Cl(OX)] is evidence that the nature of the ^{1}MLCT excited state is not significantly perturbed by substitution of the pyridine ligand.

The resonance Raman spectra of [Re(CO)$_3$Cl(DPA)] show no C≡O enhancement at any probed wavelength, which indicates negligible contributions from MLCT transitions. Spectra acquired at λ_{ex} = 444.3 nm and longer wavelengths appear very similar, corresponding to the lowest energy absorption peak found in this region. Resonance enhancement for these spectra is observed most prominently for peaks at 1031, 1179, 1192, 1540, and 1586 cm^{-1}. While the peaks at 1031 and 1540 cm^{-1} are due to vibrations of the bipyridine moiety, the peaks at 1179 and 1192 cm^{-1} involve vibrations of the diphenylaniline and C=C moieties. The example presented in Figure 9 shows activity in similar regions to the donor MOs, as discussed above (see Table 5). These data are consistent with an LCCT transition, best described as a transfer of an electron from the diphenylaniline to the bpy section of the ligand. The main contribution from the metal lies in conformational constraints as well as a slight electron-withdrawing effect, which leads to a red shift of this transition in the absorption spectrum when compared to [Cu(PPh$_3$)$_2$(DPA)]$^+$. At λ_{ex} = 350.7 nm, resonance enhancement occurs for the peak at 1612 cm^{-1}, corresponding to a vibration that is delocalized over the entire ligand (see Figure 9). It should be noted that this peak is distinct from peaks observed

dx.doi.org/10.1021/ic3018387 | Inorg. Chem. XXXX, XXX, XXX−XXX

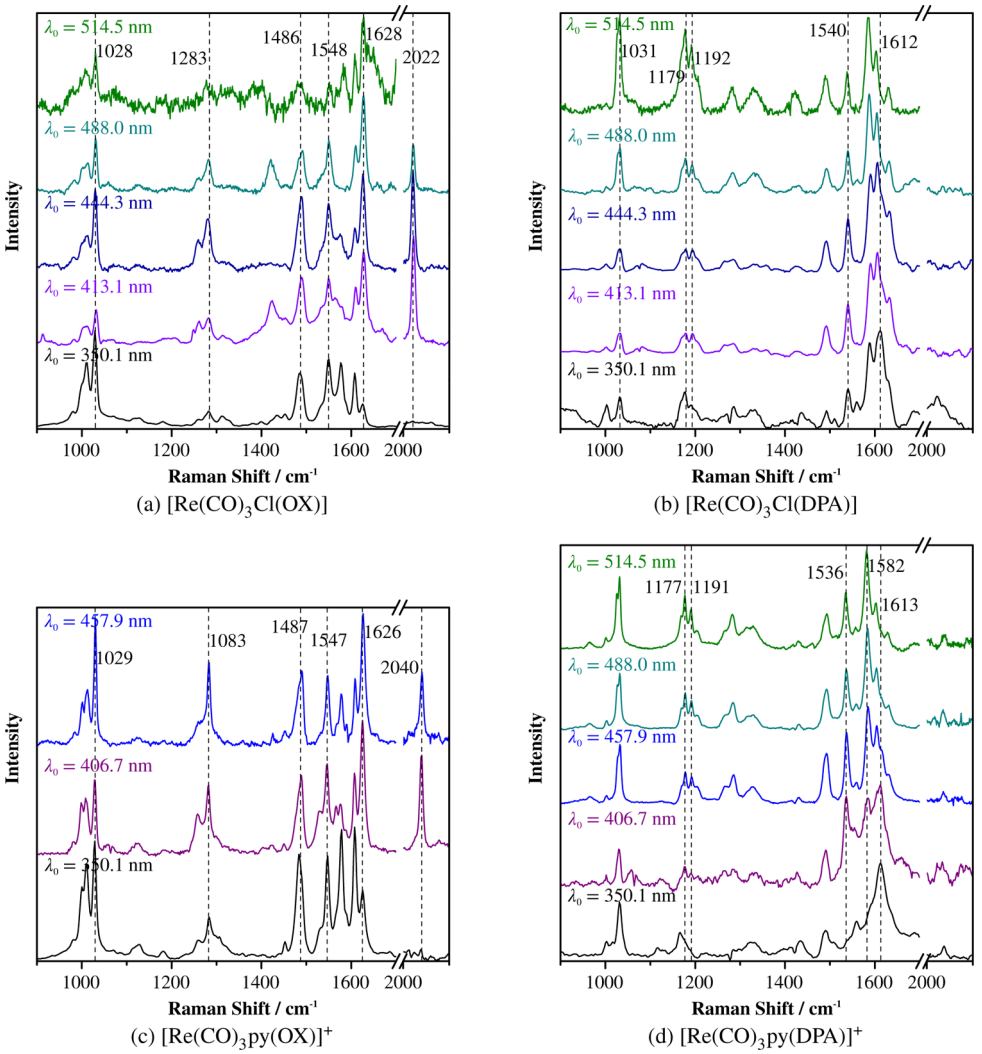

Figure 8. Resonance Raman spectra at a number of excitation wavelengths: (a) $[Re(CO)_3Cl(OX)]$ acquired in DMSO, (b) $[Re(CO)_3Cl(DPA)]$ acquired in DMSO, (c) $[Re(CO)_3py(OX)]^+$ acquired in CH_2Cl_2, (d) $[Re(CO)_3py(DPA)]^+$ acquired in CH_2Cl_2.

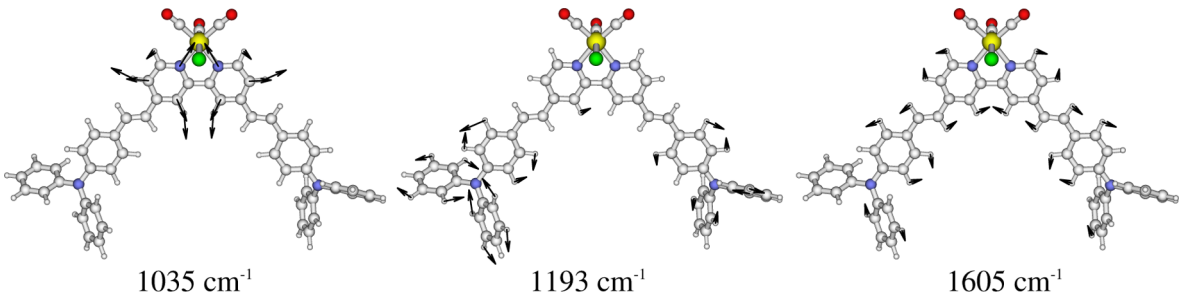

Figure 9. Examples of normal modes, with their corresponding *calculated* wavenumbers, corresponding to bpy-centered, diphenylaniline-centered, and delocalized vibrations seen in the resonance Raman spectra of $[Re(CO)_3Cl(DPA)]$.

at all other wavelengths and thus highly characteristic of the transition in this wavelength range. The peak at 376 nm in the absorption spectrum has thus been assigned as corresponding to a $\pi \rightarrow \pi^*$ transition.

Spectra of $[Re(CO)_3py(DPA)]^+$ are similar to those of $[Re(CO)_3Cl(DPA)]$, showing a similar pattern of peak enhancements. The peaks characteristic of the LCCT transition give way to the $\pi \rightarrow \pi^*$ marker bands at somewhat longer wavelengths compared to the $[Re(CO)_3Cl(NN)]$ complex, evidenced by the shoulder at 1613 cm^{-1} visible in the λ_{ex} = 457.9 nm spectrum. This is consistent with the lowering in energy of the bpy-based π_L^* orbital that acts as an acceptor during the LCCT transition, effected by the relative electron-withdrawing effect of the py ligand, as discussed above. Due to the relative distance of the diphenylaniline-based π_L^* orbital, it is expected to be less affected by the stabilizing influence of the py ligand compared to the bpy-based acceptor orbital, which is manifested in a decreased LCCT energy. Conversely, the $\pi \rightarrow \pi^*$ transition remains relatively unaffected. This is also evident from comparison of the MO energies presented in Figure 7.

dx.doi.org/10.1021/ic3018387 | Inorg. Chem. XXXX, XXX, XXX−XXX

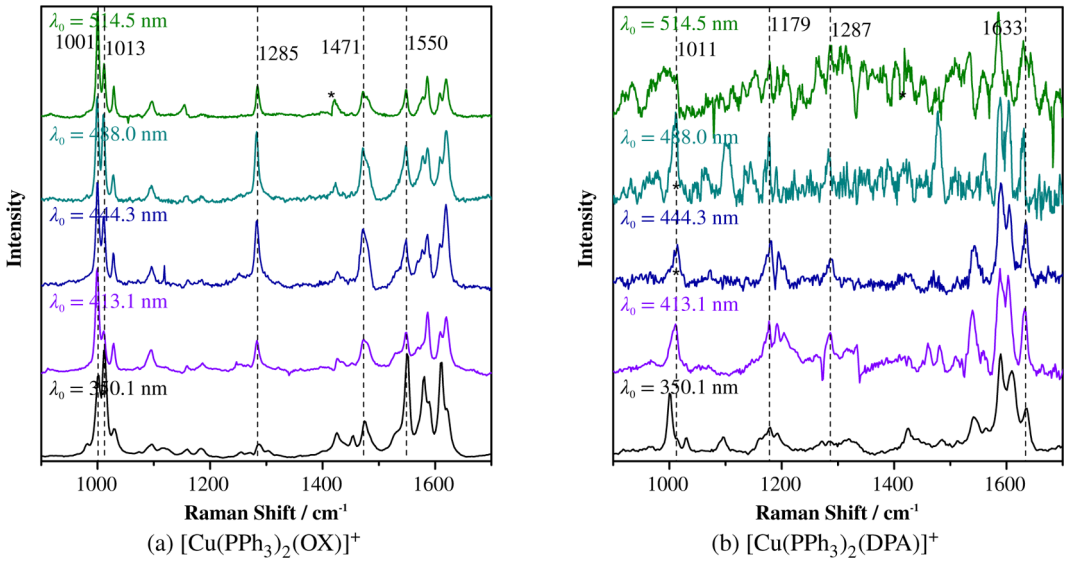

Figure 10. Resonance Raman spectra at various excitation wavelengths, acquired in CH_2Cl_2: (a) $[Cu(PPh_3)_2(OX)]^+$ and (b) $[Cu(PPh_3)_2(DPA)]^+$. Solvent subtraction has been performed. Residuals that appear are marked with asterisks.

Table 6. Summary of Emission and Transient Absorption Data[a]

		emission		transient absorption		
	solvent	λ_{max}[b]/nm	τ[c]/ns	λ_{max}[b]/nm	τ[c]/ns	assignment
$[Re(CO)_3Cl(OX)]$	CH_2Cl_2	440	<10			$^1(\pi \rightarrow \pi^*)_{bpy}$
		690	17	380, 520	21	$^3MLCT_{bpy}$
	CH_3CN			370, 525	13	$^3MLCT_{bpy}$
$[Re(CO)_3Cl(DPA)]$	CH_2Cl_2	520	<10			$^1(\pi \rightarrow \pi^*)$
				418, 555, 670	600	$LCCT_{DPA \rightarrow bpy}$
	CH_3CN	514	<10			$^1(\pi \rightarrow \pi^*)$
$[Re(CO)_3py(OX)]^+$	CH_2Cl_2	603	300	375, 506, 760	300	$^3MLCT_{bpy}$
	CH_3CN	622	90	370, 500, 740	86	$^3MLCT_{bpy}$
$[Re(CO)_3py(DPA)]^+$	CH_2Cl_2	510	<10			$^1(\pi \rightarrow \pi^*)$
				430, 640	1700	$LCCT_{DPA \rightarrow bpy}$
	CH_3CN	510	<10			$^1(\pi \rightarrow \pi^*)$
				410, 640	1000	$LCCT_{DPA \rightarrow bpy}$
$[Cu(PPh_3)_2OX]^+$	CH_2Cl_2	460	<10			PPh_3
	CH_2Cl_2	407				$^1(\pi \rightarrow \pi^*)$
				370, 620[d]	16	$^3MLCT_{bpy}$
				<350, 510[e]	20	$^3MLCT_{bpy}$
$[Cu(PPh_3)_2(DPA)]^+$	CH_2Cl_2	495	<10			$^1(\pi \rightarrow \pi^*)$
		620	<10			$LCCT_{DPA \rightarrow bpy}$
	CH_3CN	513	<10	370, 490		$^1(\pi \rightarrow \pi^*)$
				580, 650	260	$LCCT_{DPA \rightarrow bpy}$

[a]All measurements are at 293 K in deaerated solvents with excitation at 350.0−354.7 nm. [b]Errors are ±20 nm. [c]Errors are ±10%. [d]Excess PPh_3 added. [e]No PPh_3 added.

At λ_{ex} = 514.5 nm, the RR spectrum of $[Cu(PPh_3)_2(OX)]^+$ appears very similar to the FT-Raman spectrum and indeed the FT-Raman spectrum of $[Cu(PPh_3)_2(bpy)]^+$ (see Figure S2, Supporting Information). Some resonance enhancement is observed for peaks at 1001, 1285, and 1471 cm^{-1}, which are assigned as bipyridine vibrations from the frequency calculation. This is very similar up to excitation energies of 413.1 nm. At λ_{ex} = 350.7 nm the peaks at 1013 and 1550 cm^{-1} are significantly enhanced, and these are both identified as delocalized vibrations involving the entire ligand. Identification is somewhat ambiguous for the latter peak, as there is significant activity in that part of the calculated spectrum; however, most of this activity is due to various delocalized modes, giving some confidence to the assignment. Furthermore, a similar peak is absent in the FT-Raman spectrum of $[Cu(PPh_3)_2(bpy)]^+$. This is evidence for a MLCT transition at 437 nm in the absorption spectrum and a $\pi \rightarrow \pi^*$ transition at short wavelengths, similar to $[Re(CO)_3Cl(bpy)]$.

Due to significant fluorescence, the signal-to-noise ratio for complex $[Cu(PPh_3)_2(DPA)]^+$ becomes prohibitively small at λ_{ex} > 488.0 nm, and therefore, spectra acquired at higher wavelengths are omitted from analysis. Visible in all spectra but diminishing for λ_{ex} = 350.7 nm are vinyl stretching peaks at 1633 cm^{-1}. Also observed at longer wavelengths are peaks at

dx.doi.org/10.1021/ic3018387 | Inorg. Chem. XXXX, XXX, XXX−XXX

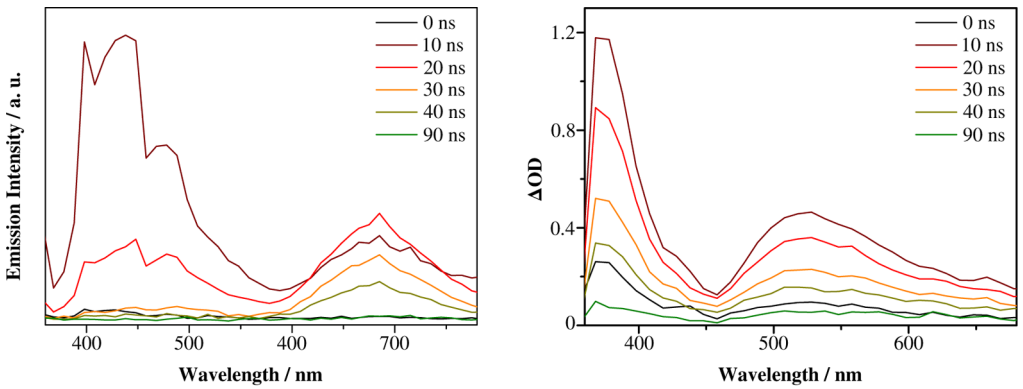

(a) $[Re(CO)_3Cl(OX)]$ transient emission (b) $[Re(CO)_3Cl(OX)]$ transient absorption

Figure 11. (a) Transient emission and (b) transient absorption spectra of $[Re(CO)_3Cl(OX)]$ in deaerated CH_2Cl_2 at room temperature.

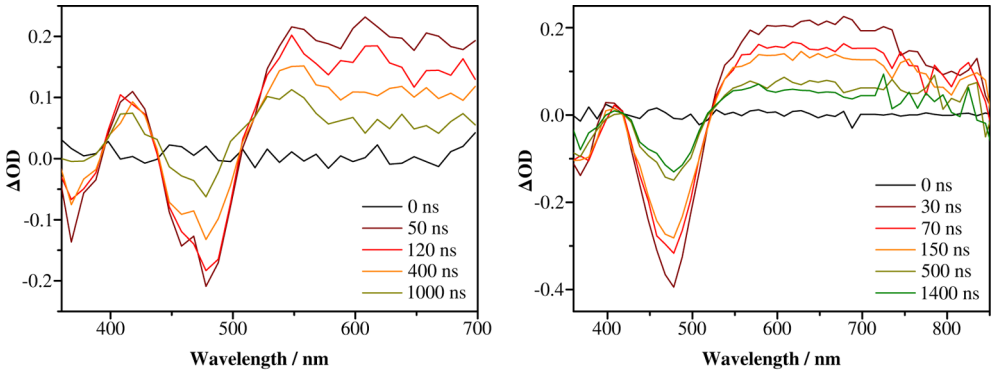

(a) $[Re(CO)_3Cl(DPA)]$ transient absorption (b) $[Re(CO)_3py(DPA)]^+$ transient absorption

Figure 12. Transient absorption spectra of (a) $[Re(CO)_3Cl(DPA)]$ in deaerated CH_2Cl_2 and (b) $[Re(CO)_3py(DPA)]^+$ in deaerated CH_3CN at room temperature.

1179 and 1287 cm^{-1}, which are assigned as diphenylaniline-based and bpy-based, respectively. This is evidence for an LCCT transition, as concluded for the rhenium complexes and predicted by TD-DFT. At λ_{ex} = 350.7 nm, the spectrum is dominated by peaks at 1589 and 1609 cm^{-1}.

In summary, the resonance Raman data show that the lowest energy transitions of complexes with the OX ligand are MLCT in nature, similar to the bpy complexes, albeit at lower energies due to the electron-withdrawing nature of the oxadiazole groups and increase in conjugation length. The electron-donating nature of the diphenylaniline group effects compounds with the DPA ligand to undergo ligand-centered charge transfer as their lowest energy electronic transition. The regions of activity predicted by calculated MOs match those observed in the resonance Raman experiments. MLCT transitions could not be detected for these compounds, as evidenced by the lack of carbonyl peaks for rhenium DPA complexes; they are potentially masked by the stronger intraligand transitions. This is consistent with electronic data and TD-DFT calculations presented above.

Excited-State Electronic Spectroscopy. Transient absorption and emission data are summarized in Table 6, and representative examples of acquired data are shown in Figures 11 and 12.

Due to the high photon flux of the pump laser, photochemical effects such as conformational changes were observed for some samples. A number of steps were taken to prevent or elucidate these effects. Acquisitions were repeated several times using different samples, and changes were monitored by carrying out electronic absorption measurements before and after pulse laser irradiation. All samples were thoroughly degassed with dry argon to remove dissolved oxygen, and the temperature was held constant at 293 K. For the $[Re(CO)_3Cl(NN)]$ complexes, a prevalent mode of breakdown was thought to be via loss of Cl^-. A potential monitor for this is to carry out experiments in CH_3CN, which is a much more strongly coordinating solvent than CH_2Cl_2 and should thus exacerbate any such effects. Conversely, as py is expected to be much more strongly coordinating than Cl^-, the $[Re(CO)_3py(NN)]^+$ complexes represent a step toward increased stability.

As shown in Figure 11, $[Re(CO)_3Cl(OX)]$ shows two emission transients. A short-lived band (τ < 10 ns) at 440 nm is assigned to a radiative decay of the intraligand $^1(\pi \rightarrow \pi^*)_{bpy}$ state. No corresponding transient absorption peaks were observed. A lower energy band is found at 690 nm, the corresponding state of which possesses a lifetime of 17 ns. This has been assigned to the radiative decay of a $^3MLCT_{bpy}$ state. However, some mixing with a $Cl^- \rightarrow$ bpy intraligand charge transfer (ILCT) state is expected.[41] In comparison, unsubstituted $[Re(CO)_3Cl(bpy)]$ shows an emission band at 622 nm corresponding to a state with a lifetime of 51 ns (in methylene chloride).[12] The observed red shift of this band of ca. 70 nm represents a decrease in the energy of the thermally equilibrated excited (THEXI) state, effected by the electron-withdrawing oxadiazole substituent. Working under the assumption that $\Delta E \approx E_{em}$, where ΔE is the energy gap between ground and excited

dx.doi.org/10.1021/ic3018387 | Inorg. Chem. XXXX, XXX, XXX–XXX

states and E_{em} is the emission energy, the decreased emission lifetime compared to unsubstituted $[Re(CO)_3Cl(bpy)]$[1,10,12] is consistent with the energy gap law.[1,12,42] In other words, a smaller ΔE leads to increased overlap between ground and excited states and thus an increased rate of nonradiative decay. It should be pointed out that the Stokes shift of this complex is actually decreased with respect to $[Re(CO)_3Cl(bpy)]$ (8400 compared to 9800 cm^{-1}) (measured as the difference between the peak of the absorption band to the peak of the emission band), indicating that ΔQ, the change in equilibrium bond lengths, is smaller for $[Re(CO)_3Cl(OX)]$. This makes sense when considering that the excited electron would be delocalized over a larger and more electrophilic ligand compared to the bpy complex. Emission decay from the lower energy state appears at a time slightly delayed with respect to the high-energy band, indicating some $(\pi \rightarrow \pi^*)_{bpy} \rightarrow {}^3MLCT_{bpy}$ conversion. Transient absorption peaks of $[Re(CO)_3Cl(OX)]$ are observed at 380 and 520 nm and show similar lifetimes to the emissive ^{3}MLCT state. Both bands are assigned as $\pi \rightarrow \pi^*$ transitions of the radical anion of bpy, analogous to $[Re(CO)_3Cl(bpy)]$[43] and consistent with absorption peaks observed at 380 and 440 nm in chemically reduced bpy.[44] The lower energy band appears affected by the oxadiazole substituent, as indicated by a red shift compared to $[Re(CO)_3Cl(bpy)]$. In CH_3CN, the emission is quenched and the lifetime of the transient absorption peaks is reduced to close to the duration of the laser pulse; however, the observed peak positions remain the same.

Changing the Cl^- ligand to py changes the excited-state kinetics but not the nature of the lowest energy excited state accessed, which is again assigned as $^3MLCT_{bpy}$. In CH_2Cl_2 an emission peak is observed, centered at 603 nm, with a lifetime of 300 ns. Blue-shifted emission compared to $[Re(CO)_3Cl(OX)]$ is consistent with an increased energy gap between the $d\pi$ and the π_L orbitals, as discussed above (see Figure 7). The Stokes shift increases slightly, to 8700 cm^{-1}. The increase in excited-state lifetime is comparable to that observed for $[Re(CO)_3Cl(bpy)]$ compared to $[Re(CO)_3py(bpy)]^+$ (51 ns compared to 669 ns in methylene chloride)[12] and is consistent with the change in ΔE. The mechanism for the large increase in lifetime has also been rationalized by decreased ILCT mixing expected for this state, due to an increased energy gap between $d\pi$ and π_L orbitals compared to the $[Re(CO)_3Cl(NN)]$ complex.[41,45] Unlike $[Re(CO)_3Cl(OX)]$, $[Re(CO)_3py(OX)]^+$ shows no obvious high-energy $(\pi \rightarrow \pi^*)_{bpy}$ emission. However, it should be noted that the initial phase of the observed emission is best modeled by including a second transient with a lifetime of 26 ns (cf. the low-energy band in Figure 11a), which is possibly due to such a state. An observed blue shift in emission is consistent with a lowering in energy of the metal $d\pi$ orbitals with substitution of the more electronegative py ligand. This shift is on the order of 2100 cm^{-1}, compared with 2500 cm^{-1} for the lowest energy absorption peaks of these complexes, indicating similar levels of communication of the metal with the FC and THEXI states of the complex. In CH_3CN the transient lifetime is decreased to 90 ns and the emission red shifted to 622 nm; this solvatochromic shift is a consequence of increased stabilization of the THEXI state by the higher polarity of the solvent. Again, the relationship between ΔE and τ is qualitatively consistent with the energy gap law. The transient absorption peaks at 375 and 506 nm, which are comparable to those of $[Re(CO)_3Cl(OX)]$, are assigned as $\pi \rightarrow \pi^*$ transitions of the radical anion of bpy. In addition to these peaks, a broad low-energy peak is also observed at 760 nm (~13 000 cm^{-1}). Ground-state calculations suggest an energy difference between the LUMO and the lowest unoccupied py orbital of ~12 000 cm^{-1}. Assuming the MO energies show little relative variation during excitation, an assignment that is energetically reasonable would be a $^3MLCT_{bpy} \rightarrow {}^3MLCT_{py}$ or $^3MLCT_{bpy} \rightarrow (\pi \rightarrow \pi^*)_{py}$ transition, that is, a transition involving an electron shift from bpy to py. Such processes have been shown to occur spontaneously for $[Re(CO)_3L(bpy)]^+$, where L is 1,2-bis(4-pyridyl)ethylene or *trans*-4-styrylpyridine, using time-resolved infrared (TRIR) measurements.[46,47] Due to the increased reduction potential of py compared to these ligands, this transition would be optically driven in $[Re(CO)_3py(OX)]^+$ instead. An electron transfer from the Cl^- ligand to the Re metal is unlikely, as it has been observed for $[Re(CO)_3Cl(bpy)]$ at 510 nm,[43] and given the relative electron withdrawing nature of py, this transition is not expected to shift to lower energies. As with $[Re(CO)_3Cl(OX)]$, a decreased transient lifetime is observed in CH_3CN.

$[Cu(PPh_3)_2(OX)]^+$ shows very low signal-to-noise ratios for both transient absorption and emission measurements. However, it has been possible to observe some transient states. A short-lived and weak emission peak was seen at 460 nm. Using the high-sensitivity resonance Raman detector a variable-temperature emission experiment was carried out. At 253 K, a peak at 407 nm was observed, which decreased in intensity as the temperature was increased, diminishing sufficiently at 305 K to show a prominent shoulder at 470 nm. No appreciable shift in the peak positions was observed. Addition of excess PPh_3 significantly enhanced the intensity of the low-energy peak. Luminescence of PPh_3 (or impurities therein) has previously been observed at 450 nm[48] (in ethanol), and we therefore assign the short-lived peak at 470 nm to this species. The peak at 407 nm is tentatively assigned as radiative decay of a $^1(\pi \rightarrow \pi^*)_{bpy}$ state, analogous to the high-energy decay observed for $[Re(CO)_3Cl(OX)]$. Weak transient absorption bands at 370 and 620 nm are observed ($\tau \approx 16$ ns) when excess PPh_3 is added to the solution and at <350 and 510 nm ($\tau \approx 20$ ns) with no PPh_3 present. The compound was found to break down immediately when dissolved in CH_3CN, as evidenced by complete discoloration and changes in the absorption spectrum. No attempt to acquire excited-state data was therefore made in this solvent.

$[Re(CO)_3Cl(DPA)]$ shows an emission peak, with a lifetime shorter than the laser pulse (~7 ns), centered at 520 nm. As mentioned below, emission from the free ligand occurs at 495 nm (in CH_2Cl_2); thus, this is consistent with prompt fluorescence from a $^1(\pi \rightarrow \pi^*)$ state. Transient absorption data show a number of peaks belonging to a dark state, with a comparatively long lifetime of 600 ns. Two peaks are visible, at ca. 555 and 670 nm, and part of a broad transient that stretches to the red edge of the window (Figure 12a). Unlike the OX-based complexes, depletions of the ground state, corresponding to the presence of absorption peaks in the ground-state absorption spectrum, are also observed with matching lifetimes. The relatively long excited-state lifetime is inconsistent with ^{3}MLCT states of complexes of the type $Re(CO)_3Cl(L)$ (where L = polypyridyl). Furthermore, there is no evidence for a strong absorption at ca. 380 nm that has been used as evidence for the presence of the radical anion of bpy.[49,50] The nature of the THEXI state can therefore be concluded to be either $^3(\pi \rightarrow \pi^*)$ or LCCT. MO pictures from triplet-state calculations (see Figure 13 for an example involving $[Re(CO)_3Cl(DPA)]^+$)

dx.doi.org/10.1021/ic3018387 | Inorg. Chem. XXXX, XXX, XXX–XXX

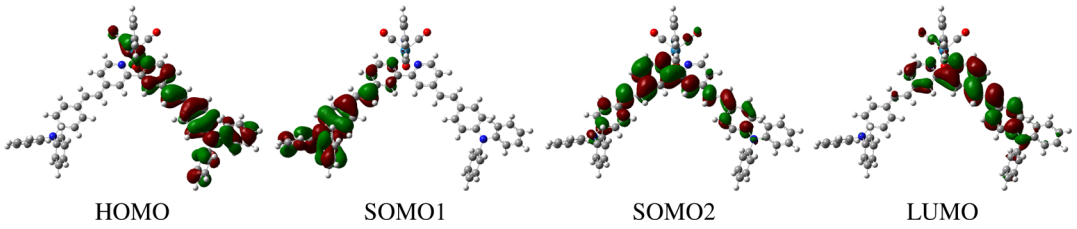

Figure 13. MO pictures of the highest occupied, partially occupied, and lowest unoccupied molecular orbitals of the calculated triplet state (using B3LYP) of $[Re(CO)_3py(DPA)]^+$.

show singly occupied molecular orbitals (SOMOs) that are diphenylaniline and bpy based, which is consistent with a THEXI state that is LCCT in nature. One should note that the LCCT state is *not charge separated*; both the donor and the acceptor orbitals have overlap and thus appreciable $^3(\pi \rightarrow \pi^*)$ character. A number of good examples of charge-separated states have been studied, and they are characterized with short-lived excited states which show electron tunneling through spacer groups[51,52] which are not present in $[Re(CO)_3Cl(DPA)]^+$

While the SOMOs of the Cl^- and py complexes appear almost identical, the HOMO of the former is metal based (not shown), which is consistent with a smaller energy gap between the dπ and the π_L orbitals. As can be seen from Figure 12a, the transients of the peaks at 418 and 555 nm persist for longer than depletion of the ground state. This is not inconsistent with a cis/trans isomerization of one of the C=C groups. While none of the cis product has been isolated, an electronic transition of this species has been calculated using TD-DFT at ca. 540 nm, which points to a retained ΔOD in this spectral region. It appears that the trans isomer reforms over a period of minutes as no permanent photoproduct can be observed. In CH_3CN this complex undergoes photochemical reactions upon excitation, thus precluding analysis of the transient absorption data. However, short-lived emission has been observed at 514 nm, which will be further discussed in reference to the copper complex below.

The py complexes are stable in both CH_2Cl_2 and CH_3CN; an example of transient absorption spectra in the latter solvent is presented in Figure 12b. The low-energy band is somewhat broader than for $[Re(CO)_3Cl(DPA)]$, and individual peaks can no longer be assigned. However, the spectra bear many similarities otherwise. Most importantly, the excited-state lifetime of the dark state increases to 1700 and 1000 ns in CH_2Cl_2 and CH_3CN, respectively. This is most likely an effect of communication with a ^{3}MLCT state of similar energy in the $[Re(CO)_3Cl(NN)]$ complex,[45] facilitating deactivation via the $a'(1)$ vibrational mode of the $\{Re(CO)_3Cl\}$ moiety. This mode has been identified as a major energy acceptor in the nonradiative deactivation of $[Re(CO)_3Cl(bpy)]$ complexes.[12,53] The level of communication and associated excited-state deactivation would be expected to be decreased for $[Re(CO)_3py(DPA)]^+$ due to the aforementioned increase in separation between the dπ and the π_L orbitals. The calculated separation between the highest energy occupied dπ orbital and the singly occupied π_L orbital in the triplet state is ca. 13 300 and 7900 cm^{-1} for $[Re(CO)_3py(DPA)]$ and $[Re(CO)_3Cl(DPA)]$, respectively. MO pictures of the calculated triplet state clearly show the LCCT nature of this state (Figure 13).

Two short-lived emission peaks are observed for $[Cu(PPh_3)_2(DPA)]^+$ in CH_2Cl_2 at 495 and 620 nm. The former dominates when excess PPh_3 is added; however, strong emission at 620 nm can still be observed if the solution is excited at 450 nm. It is known that the ligand absorbs at 395 nm and emits strongly at 475 nm (on a glass substrate),[22] which is consistent with the observed high-energy emission peak. Thus, if addition of excess PPh_3 causes the following equilibrium[24] to shift to the right

$$[Cu(DPA)(PPh_3)_2]^+ + 2PPh_3 \rightleftharpoons [Cu(PPh_3)_4]^+ + DPA$$

it is likely that the observed high-energy emission stems from free ligand in solution. Any remaining ligand bound to copper will absorb 450 nm light and emit at 620 nm, and thus, the low-energy emission band is assigned as LCCT based. A solution of $[Cu(PPh_3)_2(DPA)]^+$ in CH_3CN is highly emissive, with a peak at 513 nm. This is probably due to emission of free ligand in CH_3CN; use of a coordinating solvent causes more ligand to be liberated. No transient absorption signals could be obtained from $[Cu(PPh_3)_2(DPA)]^+$ in CH_2Cl_2. However, ground-state depletion is observed at 430 nm when the experiment is carried out in CH_3CN, along with grow-in of a broad band with two peaks at ca. 580 and 650 nm.

In summary, the OX complexes possess a THEXI state that is $^3MLCT_{bpy}$ in nature. This state is relatively short lived for $[Re(CO)_3Cl(OX)]$ and $[Cu(PPh_3)_2(OX)]^+$ and, where observable, decreases in lifetime in CH_3CN, a higher polarity solvent. $[Re(CO)_3Cl(OX)]$ shows a lifetime of 300 ns, which decreases to ca. 90 ns in CH_3CN. Complexes based on the DPA ligand show dark excited states that are considerably longer lived compared to either unsubstituted or oxadiazole-substituted $[Re(CO)_3Cl(bpy)]$. Due to the important role of the $\{Re(CO)_3Cl\}$ unit in nonradiative excited-state deactivation, this suggests an excited state that is mostly ligand based, an assignment that is supported by triplet-state DFT calculations.

CONCLUSION

We synthesized rhenium and copper complexes of ligands bpy, OX, and DPA and investigated their photophysical properties. The crystal structure of $[Re(CO)_3Cl(DPA)]$ confirms the trans arrangement of the ethylene bonds. The $[Cu(PPh_3)_2(OX)]^+$ structure shows that the oxadiazole ligand adopts a near planar arrangement. Electronic absorption and resonance Raman suggest that the oxadiazole-substituted complexes undergo MLCT excitation at slightly longer wavelengths than the unsubstituted complexes, which is consistent with previous observations. Conversely, the DPA complexes show a strong absorption peak in the visible region, which has been assigned, using resonance Raman to a LCCT transition involving the diphenylaniline and bpy as donor and acceptor units, respectively. A lack of carbonyl stretches suggests this transition is entirely located on the DPA ligand. Relevant calculated MOs are consistent with these data. Excited states of these complexes

dx.doi.org/10.1021/ic3018387 | Inorg. Chem. XXXX, XXX, XXX−XXX

were probed using transient absorption and emission spectroscopic techniques. Short-lived $^1(\pi \rightarrow \pi^*)$ transitions were found for a number of complexes. The THEXI states of the OX complexes have been assigned as ^{3}MLCT, while the DPA compounds showed relatively long-lived dark states. For the latter, attachment of a metal has a detrimental effect on the luminescence. Consistent with triplet-state DFT calculations, the dark states have been assigned as LCCT in nature; their lifetimes are consistent with excited states that experience relatively little influence from the attatched metals, which serve essentially as conformational constraints.

■ ASSOCIATED CONTENT

Supporting Information

Additional crystal structures, MADs, and scale factors of calculated vibrations, FT-Raman spectra of bpy complexes, transient absorption data and emission spectra of $[Re(CO)_3py(OX)]^+$, and additional MO diagrams. This material is available free of charge via the Internet at http://pubs.acs.org.

■ AUTHOR INFORMATION

Corresponding Author

*E-mail: keith.gordon@otago.ac.nz.

Notes

The authors declare no competing financial interest.

■ REFERENCES

(1) Worl, L. A.; Duesing, R.; Chen, P.; Della Ciana, L.; Meyer, T. J. *J. Chem. Soc., Dalton Trans.* **1991**, 849−858.
(2) Shirota, Y.; Kageyama, H. *Chem. Rev.* **2007**, *107*, 953−1010.
(3) Lundin, N. J.; Blackman, A. G.; Gordon, K. C.; Officer, D. L. *Angew. Chem., Int. Ed.* **2006**, *45*, 2582−2584.
(4) Easun, T. L.; Alsindi, W. Z.; Towrie, M.; Ronayne, K. L.; Sun, X.-Z.; Ward, M. D.; George, M. W. *Inorg. Chem.* **2008**, *47*, 5071−5078.
(5) Chen, J.-L.; Cao, X.-F.; Gu, W.; Su, B.-T.; Zhang, F.; Wen, H.-R.; Hong, R. *Inorg. Chem. Commun.* **2012**, *15*, 65−68.
(6) Elliott, A. B. S.; Horvath, R.; Gordon, K. C. *Chem. Soc. Rev.* **2012**, *41*, 1929−1946.
(7) Zhang, Q.; Zhou, Q.; Cheng, Y.; Wang, L.; Ma, D.; Jing, X.; Wang, F. *Adv. Mater.* **2004**, *16*, 432−436.
(8) Zhang, Q.; Ding, J.; Cheng, Y.; Wang, L.; Xie, Z.; Jing, X.; Wang, F. *Adv. Funct. Mater.* **2007**, *17*, 2983−2990.
(9) Smothers, W. K.; Wrighton, M. S. *J. Am. Chem. Soc.* **1983**, *105*, 1067−1069.
(10) Walters, K. A.; Kim, Y.-J.; Hupp, J. T. *Inorg. Chem.* **2002**, *41*, 2909−2919.
(11) Gamelin, D. R.; George, M. W.; Glyn, P.; Grevels, F.-W.; Johnson, F. P. A.; Klotzbuecher, W.; Morrison, S. L.; Russell, G.; Schaffner, K.; Turner, J. J. *Inorg. Chem.* **1994**, *33*, 3246−3250.
(12) Caspar, J. V.; Meyer, T. J. *J. Phys. Chem.* **1983**, *87*, 952−957.
(13) Kim, Y.; Vanhelmont, F. W. M.; Stern, C. L.; Hupp, J. T. *Inorg. Chim. Acta* **2001**, *318*, 53−60.
(14) Lundin, N. J.; Walsh, P. J.; Howell, S. L.; Blackman, A. G.; Gordon, K. C. *Chem.−Eur. J.* **2008**, *14*, 11573−11583.
(15) Ng, P. K.; Gong, X.; Chan, S. H.; Lam, L. S. M.; Chan, W. K. *Chem.−Eur. J.* **2001**, *7*, 4358−4367.
(16) Karthikeyan, C. S.; Wietasch, H.; Thelakkat, M. *Adv. Mater.* **2007**, *19*, 1091−1095.
(17) Giribabu, L.; Bessho, T.; Srinivasu, M.; Vijaykumar, C.; Soujanya, Y.; Reddy, V. G.; Reddy, P. Y.; Yum, J.-H.; Gratzel, M.; Nazeeruddin, M. K. *Dalton Trans.* **2011**, *40*, 4497−4504.
(18) Bandara, J.; Willinger, K.; Thelakkat, M. *Phys. Chem. Chem. Phys.* **2011**, *13*, 12906−12911.
(19) Willinger, K.; Fischer, K.; Kisselev, R.; Thelakkat, M. *J. Mater. Chem.* **2009**, *19*, 5364−5376.
(20) Myahkostupov, M.; Castellano, F. N. *Inorg. Chem.* **2011**, *50*, 9714−9727.
(21) Fraser, M. G.; Clark, C. A.; Horvath, R.; Lind, S. J.; Blackman, A. G.; Sun, X.-Z.; George, M. W.; Gordon, K. C. *Inorg. Chem.* **2011**, *50*, 6093−6106.
(22) Kay, K. Y.; Cho, S. Y.; Park, H. C.; Park, J. W. *Synth. Met.* **2003**, *137*, 1045−1046.
(23) Lundin, N. J.; Walsh, P. J.; Howell, S. L.; McGarvey, J. J.; Blackman, A. G.; Gordon, K. C. *Inorg. Chem.* **2005**, *44*, 3551−3560.
(24) Rader, R. A.; McMillin, D. R.; Buckner, M. T.; Matthews, T. G.; Casadonte, D. J.; Lengel, R. K.; Whittaker, S. B.; Darmon, L. M.; Lytle, F. E. *J. Am. Chem. Soc.* **1981**, *103*, 5906−5912.
(25) Kilpin, K. J.; Horvath, R.; Jameson, G. B.; Telfer, S. G.; Gordon, K. C.; Crowley, J. D. *Organometallics* **2010**, *29*, 6186−6195.
(26) Howell, S. L.; Matthewson, B. J.; Polson, M. I. J.; Burrell, A. K.; Gordon, K. C. *Inorg. Chem.* **2004**, *43*, 2876−2887.
(27) Howell, S. L.; Gordon, K. C. *J. Phys. Chem. A* **2004**, *108*, 2536−2544.
(28) Howell, S. L.; Gordon, K. C.; McGarvey, J. J. *J. Phys. Chem. A* **2005**, *109*, 2948−2956.
(29) Fraser, M. G.; Blackman, A. G.; Irwin, G. I. S.; Easton, C. P.; Gordon, K. C. *Inorg. Chem.* **2010**, *49*, 5180−5189.
(30) Walsh, P. J.; Gordon, K. C.; Lundin, N. J.; Blackman, A. G. *J. Phys. Chem. A* **2005**, *109*, 5933−5942.
(31) Schaftenaar, G.; Noordik, J. H. *J. Comput.-Aided Mol. Des.* **2000**, *14*, 123−134.
(32) O'Boyle, N. M.; Tenderholt, A. L.; Langner, K. M. *J. Comput. Chem.* **2008**, *29*, 839−845.
(33) Gerlits, O. O.; Coppens, P. *Acta Crystallogr. E* **2001**, *57*, m164−m166.
(34) Wenger, O. S.; Henling, L. M.; Day, M. W.; Winkler, J. R.; Gray, H. B. *Polyhedron* **2004**, *23*, 2955−2958.
(35) Yang, L.; Powell, D. R.; Houser, R. P. *Dalton Trans.* **2007**, 955−964.
(36) Horvath, R.; Gordon, K. C. *Coord. Chem. Rev.* **2010**, *254*, 2505−2518.
(37) Howell, S. L.; Gordon, K. C. *J. Phys. Chem. A* **2006**, *110*, 4880−4887.
(38) Vlček, A., Jr.; Záliš, S. *Coord. Chem. Rev.* **2007**, *251*, 258−287.
(39) Yanai, T.; Tew, D. P.; Handy, N. C. *Chem. Phys. Lett.* **2004**, *393*, 51−57.
(40) Hirakawa, A. Y.; Tsuboi, M. *Science* **1975**, *188*, 359−361.
(41) Rossenaar, B. D.; Stufkens, D. J.; Vlček, A., Jr. *Inorg. Chem.* **1996**, *35*, 2902−2900.
(42) Caspar, J. V.; Kober, E. M.; Sullivan, B. P.; Meyer, T. J. *J. Am. Chem. Soc.* **1982**, *104*, 630−632.
(43) Liard, D. J.; Busby, M.; Matousek, P.; Towrie, M.; Vlček, A., Jr. *J. Phys. Chem. A* **2004**, *108*, 2363−2369.
(44) Noble, B. C.; Peacock, R. D. *Spectrochim. Acta A* **1990**, *46*, 407−412.
(45) Vlček Jr., A. *Topics in Organometallic Chemistry*; Springer: Berlin/Heidelberg, 2010; Vol. *29*, pp 115−1588.
(46) Busby, M.; Matousek, P.; Towrie, M.; Vlček, A., Jr. *J. Phys. Chem. A* **2005**, *109*, 3000−3008.
(47) Polo, A. S.; Itokazu, M. K.; Frin, K. M.; Patrocinio, A. O. d. T.; Murakami Iha, N. Y. *Coord. Chem. Rev.* **2006**, *250*, 1669−1680.
(48) Buckner, M. T.; McMillin, D. R. *J. Chem. Soc., Chem. Commun.* **1978**, 759−761.
(49) Creutz, C.; Chou, M.; Netzel, T. L.; Okumura, M.; Sutin, N. *J. Am. Chem. Soc.* **1980**, *102*, 1309−1319.
(50) Wolcan, E.; Torchia, G.; Tocho, J.; Piro, O. E.; Juliarena, P.; Ruiz, G.; Feliz, M. R. *J. Chem. Soc., Dalton Trans.* **2002**, 2194−2202.
(51) Walther, M. E.; Grilj, J.; Hanss, D.; Vauthey, E.; Wenger, O. S. *Eur. J. Inorg. Chem.* **2010**, 4843−4850.
(52) Hanss, D.; Wenger, O. S. *Inorg. Chem.* **2009**, *48*, 671.
(53) Baiano, J. A.; Murphy, J.; Rorer, W. *Inorg. Chem.* **1991**, *30*, 4594−4598.